Influence of the substrate on the overall sensor impedance of planar H$_2$ sensors involving TiO$_2$–SnO$_2$ interfaces

L. Ebersberger and G. Fischerauer

Chair of Metrology and Control Engineering, Universität Bayreuth, Bayreuth, Germany

Correspondence to: L. Ebersberger (mrt@uni-bayreuth.de)

Abstract. To date, very little has been written about the influence of the substrate layer on the overall sensor impedance of single- and multilayer planar sensors (e.g., metal-oxide sensors). However, the substrate is an elementary part of the sensor element. Through the selection of a substrate, the sensor performance can be manipulated. The current contribution reports on the substrate influence in multilayer metal-oxide chemical sensors. Measurements of the impedance are used to discuss the sensor performance with quartz substrates, (laboratory) glass substrates and substrates covered by silicon-dioxide insulating layers. Numerical experiments based on previous measurement results show that inexpensive glass substrates contribute up to 97 % to the overall sensor responses. With an isolating layer of 200 nm SiO$_2$, the glass substrate contribution is reduced to about 25 %.

1 Introduction

A metal-oxide sensor consists of a substrate (typically aluminum oxide, which, however, cannot be used for thin-film sensors owing to its high surface roughness), electrodes (typically aluminum or gold) and an active layer (differs in composition by application, mostly SnO$_2$ doped in one way or another). In the open literature, the substrate is listed as part of the sensor element (Barsan et al., 2007; Barsan and Weimar, 2001), but the research focusses on the active layer in the majority of cases and sometimes also on the electrodes. If at all, the substrate is only treated as a thermally important component (Simon et al., 2001). Rarely is it discussed with a focus on other aspects, like the influence of the substrate on the growth of the crystalline phases (Mardare et al., 2008). However, the substrate could play a decisive role in the overall impedance of the sensor system (Fischerauer et al., 2009). This contribution focusses on the influence of the substrate on the overall sensor impedance of planar (thin-film) hydrogen (H$_2$) sensors involving titanium-dioxide (TiO$_2$) stannic-dioxide (SnO$_2$) interfaces.
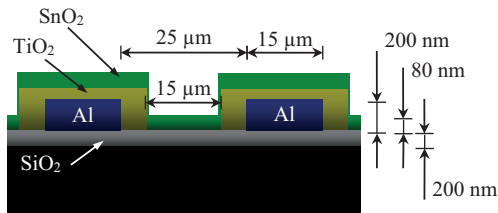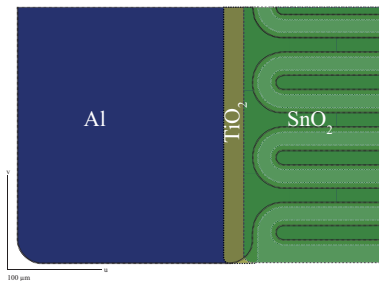
2 Sensor geometry

We have investigated three different types of sensor structures, called types A, B and C. All of them consist of planar interdigital electrodes (IDE) made of 200 nm ion-beam-deposited aluminum and respectively featuring 55 and 56 electrode fingers with a finger width of 15 µm and an interfinger space of 25 µm (Fig. 1). The finger length was 3450 µm. The substrate consisted of glass without an insulating layer (type A) or glass coated with an insulating layer of 200 nm reactive ion-beam-sputtered silicon dioxide (SiO$_2$, type B) or quartz (type C).

The 80 nm thick TiO$_2$ layer covers the top of all electrode fingers and 5 µm to their left and their right. The SnO$_2$ layer covers all electrodes, the TiO$_2$ layer and the space between the fingers (Fig. 2). A wide area of the busbar (see Fig. 2, left) is left blank for wire bonding.

The metal oxides were made by ion-beam deposition of the metals (titanium respectively tin) and thermal oxidation immediately afterwards. The oxidation was performed in a glass furnace which was heated to 500 °C in ambient atmosphere.

Table 1. Comparison between sensor types.

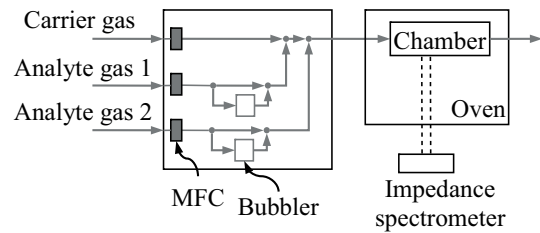|	Type A	Type B	Type C
Active layer		TiO_2-SnO_2-multilayer	
Electrodes		aluminum IDE	
Number of fingers		55/56	
Finger length		3450 µm	
Substrate	glass	glass + 200 nm SiO_2	quartz

Figure 1. Schematic cross section of the sensor structure (type B).

Figure 2. Schematic detail of the busbar area (blue: Al) and covering metal oxides (olive green: TiO_2, green: SnO_2) in a view from above. The darker parts shining through the thin films on the right-hand side are the electrode fingers.

The thermal postprocessing could lead to a doping of the active layers with aluminium from the electrodes due to the absence of a diffusion barrier layer. Furthermore, a diffusion of titanium to the tin-oxide layer (and reverse) could not be prevented. But as similar measurement results have been obtained with thermally oxidized Ti and with reactively ion-beam-sputtered TiO_2 layers, such a diffusion process appears to be insignificant.

As to the surface roughness of the metal oxides, it is caused completely by the thermal treatment of the sensors. Straight after the sputtering process the roughness was negligible and increased by the thermal oxidization.

3 Measurement setup

To characterize the sensors, they were mounted on the lower part of a DIL-14 metal case (with six grounded pins) and placed inside a measurement chamber, which in turn was placed in a temperature-controlled oven (Fig. 3). The chamber itself consisted of stainless steel and contained a base

Figure 3. Schematic drawing of the test bed used to characterize the sensors.

Figure 4. One-dimensional approximation of basis cell of an IDE-based gas sensor (type B) (Fischerauer et al., 2011).

out of Macor (Corning Inc.) which holds the metal case and contacts the pins of the sensor package. The atmosphere in the measurement chamber could be controlled via custom-specific gas-mixing equipment involving mass-flow controllers. The chamber was first heated to 270 °C in a nitrogen (N_2) atmosphere. When the steady state was reached, selected amounts of hydrogen and water were added to the nitrogen carrier gas. The temperature of 270 °C was chosen, because it is known that at least TiO_2 nanotubes are sensitive to H_2 in this temperature region (Varghese et al., 2003). The overall gas flow was held constant at 500 cm^3 min^{-1}. For lower concentration levels, the analytes were partly pre-thinned to 5 % in nitrogen carrier gas. A bubbler was used for the humidification of the gas.

The sensor response to concentration steps in hydrogen or H_2O was observed via the electrical terminals of the sensors considered as two-terminal devices. These terminal characteristics were measured by impedance spectrometers (Meodat Impspec LF HF or Agilent E4980A) in the frequency range from at least 20 Hz to 10 kHz. The frequencies were logarithmically equidistantly spaced (typically 30 points per decade).

To model the sensor element, a one-dimensional approximation with a geometry comprising two parallel tracks was used as described in Fischerauer et al. (2011) and illustrated in Fig. 4.

The overall impedance $\underline{Z}(f)$ is then calculated as

$$\underline{Z}(f) = \frac{\underline{Z}_a(f) \cdot \underline{Z}_s(f)}{\underline{Z}_a(f) + \underline{Z}_s(f)}, \tag{1}$$

where $\underline{Z}_a(f)$ denotes the impedance of the active layer and $\underline{Z}_s(f)$ is the impedance of the substrate (including insulating layers).
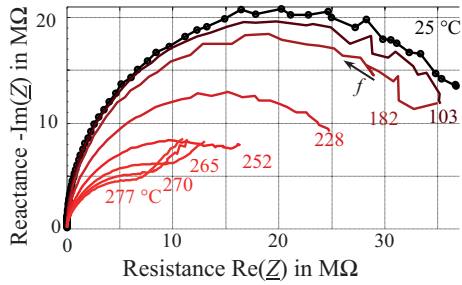
Figure 5. Nyquist plot of the measured impedance of an unbonded sensor in its test cell at various temperatures. The frequency was swept from 10.3 Hz to 10 kHz. For the temperature of 25 °C, the measurement points are also plotted. At the highest temperature, different levels of H_2 were added to the nitrogen.
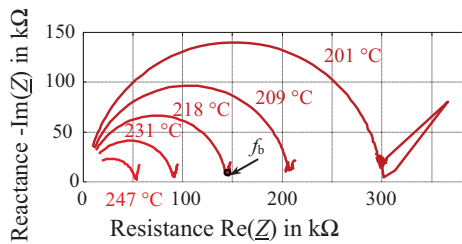

Figure 6. Nyquist plot of the measured impedance of of a type-A sensor element without active layers (pure IDE on glass substrate). Again, the frequency was swept from 10.3 Hz to 10 kHz. At the peak temperature of 247 °C H_2O was added, but produced no effect. For the 218 °C curve, the inflexion frequency f_b has been marked; it will be discussed later.

It turned out, however, that the test environment also contributed to the device response. To include this influence (as a basis for an eventual de-embedding procedure), Eq. (1) is modified to

$$\underline{Z}(f) = \frac{\underline{Z}_a(f) \cdot \underline{Z}_s(f) \cdot \underline{Z}_T(f)}{\underline{Z}_a(f) \cdot \underline{Z}_s(f) + \underline{Z}_s(f) \cdot \underline{Z}_T(f) + \underline{Z}_a(f) \cdot \underline{Z}_T(f)}, \quad (2)$$

where $\underline{Z}_T(f)$ denotes the impedance contribution of the test environment (including cable capacitances and insulator resistances). This model is solely based on the parallel connection of lumped elements and as such is quite crude. The limitations of the simple network are made up for by allowing all network elements to be frequency-dependent. This procedure is common practice in impedance spectroscopy. A more detailed mechanistic model of the test environment that would improve the correction even further is out of focus for this paper.

4 Measurement results

The measurement results will be presented in three steps. First, in Sect. 4.1, the characteristics of the bare substrate
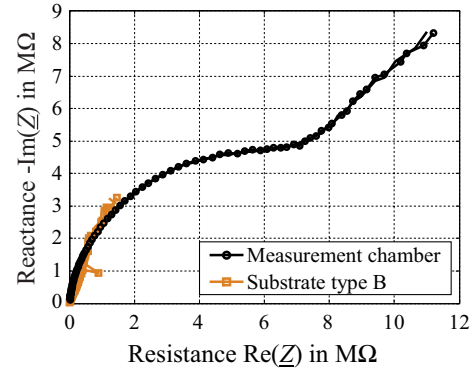

Figure 7. Comparison of type-B sensor impedance (element without any active layer) $\underline{Z}(\underline{Z}_T, \underline{Z}_{S,B})$ and the measured impedance of the empty test chamber $\underline{Z}(\underline{Z}_T)$ at an elevated temperature ($\vartheta = 280$ °C).
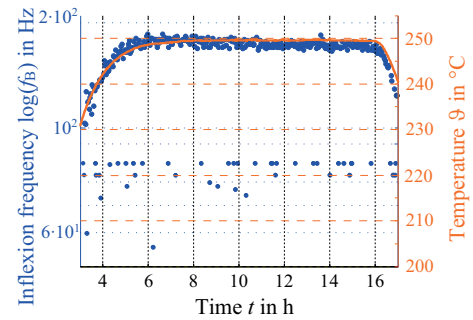

Figure 8. Time series of the inflexion frequency f_B and the temperature as measured with a thermocouple inside the measurement chamber.

will be discussed. Next, Sect. 4.2 focusses on the influence of humidity on the sensor signal. Finally, the key aspect of Sect. 4.3 is the influence of insulating layers or substrates on the sensor response.

4.1 Bare substrate

To estimate the influence of the test environment, unbonded sensors were characterized. In this manner, all aspects of the test environment (contact resistances, cable capacitances, etc.) can be quantified for later de-embedding of measurement data obtained with sensors.

As one can see in Fig. 5, even at elevated temperatures, the insulation of the chamber and the package is very high. As expected, it does not respond to H_2, which means that neither Macor nor other insulation materials are sensitive to it. In addition, neither the materials (Macor, insulating materials) nor the substrate is sensitive to H_2O. The fact, that no effect of the water is visible in Fig. 6, leads to the conclusion that none of the materials (Macor, insulation, substrate) causes an H_2O sensitivity of the sensors.
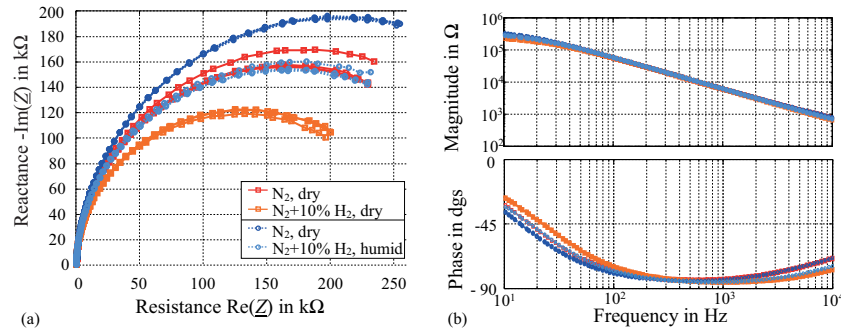
Figure 9. Measured type-B sensor impedance $\underline{Z}(\underline{Z}_T, \underline{Z}_{S,B}, \underline{Z}_a)$ in various atmospheres. All curves have been obtained with the same sensor specimen measured at various times. Case 1: N_2 with or without dry H_2 (orange and red solid lines, respectively). Case 2: N_2 with or without humid H_2 (light blue and dark blue dashed lines, respectively). Frequency from 10.3 Hz to 10 kHz. **(a)** Nyquist diagram and **(b)** Bode diagram.

As revealed by Figs. 5 and 6 , the substrate (glass) conductivity of a type-A sensor is about 100 times higher than that of the measurement environment at the same temperatures. Figure 7 demonstrates that the type-B substrate (insulated glass) leads to a slightly higher shunt conductance (parallel to the coated IDT) than the test bed alone. This means that the test bed influence can be neglected for "high-conductivity" substrates as in type-A sensors, but must be taken into account with "low-conductivity" substrates as in type-B sensors.

Apart from this, the results clearly show that a layer thickness of about 200 nm (atomic force microscopy (AFM) measurements yielded a layer thickness, for the given sensor, of 175 ± 5 nm) increases the resistivity of the substrate sufficiently.

To estimate the magnitude of the influence, we performed a numerical experiment based on measurement data for the test environment with a type-A substrate (yielding $\underline{Z}(\underline{Z}_T, \underline{Z}_{S,A})$), a type-B substrate (yielding $\underline{Z}(\underline{Z}_T, \underline{Z}_{S,B})$), and a type-B sensor (yielding $\underline{Z}(\underline{Z}_T, \underline{Z}_{S,B}, \underline{Z}_a)$) at 240 °C. The contributions of the active layer $\underline{Z}_a(f)$, the substrate A $\underline{Z}_{S,A}(f)$, the substrate B $\underline{Z}_{S,B}(f)$, and the test environment $\underline{Z}_T(f)$ were calculated by solving Eq. (2). To simulate a test gas, the impedance of the active layer $\underline{Z}_a(f)$ was increased by 100 %, leading to $\underline{Z}_{a,g}(f) = 2 \cdot \underline{Z}_a(f)$. The computations revealed that a sensor of type A would respond to this by an impedance increase of 3 % at low frequencies (10.3 Hz) and up to 92 % at high frequencies (10 kHz). In contrast, a type-B sensor would increase its impedance by 75 % at low frequencies (10.3 Hz) and 92 % at high frequencies (10 kHz). Type-C sensors would respond by even higher impedance increases. However, their low-conductivity substrate could not be measured reliably. The type-C sensors are further discussed in Sect. 4.3.

As introduced in Fischerauer and Fischerauer (2011), the inflexion frequency in the Nyquist plot of the sensor impedance (cf. Fig. 5) strongly depends on temperature. Because the dependency is non-linear, this could be used to determine the temperature of the sensor element (cf. Fig. 8).

The outliers in this plot are due to noise which perturbs the reconstruction algorithm for the inflexion frequency.

4.2   Influence of humidity

Figure 9 shows measurement results obtained for type-B sensors in various atmospheres (N_2, with dry H_2, with H_2 plus water). At first sight, one is inclined to think that the sensor resistance increases with humidity. In fact, however, humidity changes the sensor response to H_2 only very little. The seeming humidity influence is due to the baseline drift inherent to the present sensors and resulting in time-variant impedance levels. We attribute the baseline drift to aging, relaxation, poisoning or similar effects during the time interval between the measurements of cases 1 and 2 (about 6 h). Temperature fluctuations can be ruled out as source of the drift because they were held below 0.5 °C.

The assertation that humidity does not change the sensor response is corroborated by the fact that the *shape* of the Nyquist plot does not change with humidity and that characteristic quantities such as the sensor resistance, at say 10 Hz, vary with H_2 content, but not with humidity (said resistance decreases by 15 % when 10 % H_2 is added to the N_2 atmosphere).

4.3   Influence of insulating substrates

To estimate the influence of the substrate, different sensors were characterized. Figure 10 shows the results for a type-B sensor (insulated glass substrate) as compared to a type-C sensor (quartz substrate). Although the impedance level of the former is lower by about 30 %, it still is in the same range as that of the latter. The variation visible in the figure is caused by noise, not by drift. No recognizable drift could be identified during the illustrated detail, because the repeatedly measured spectra did not "move" in a specific direction.

Thus, even a thin layer of SiO_2 may suffice to make an inherently unsuitable, but inexpensive substrate (glass) suitable
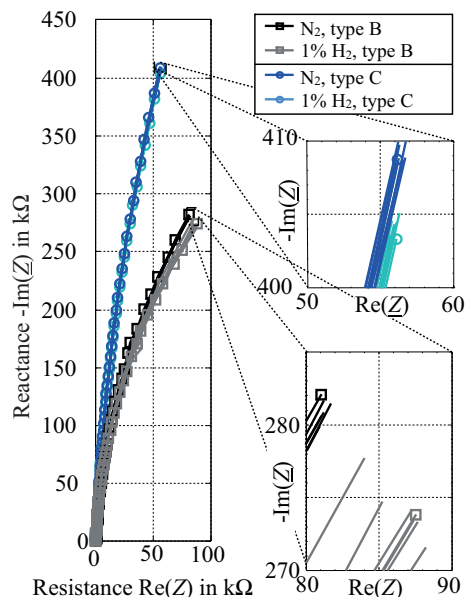
Figure 10. Measured impedances of a type-B sensor (squares) and a type-C sensor (circles). The dark symbols refer to measurement in pure N_2 repeated 7 times for each sensor type. The light symbols to measurement in N_2 plus 1 % H_2 (also repeated 7 times). Frequency from 20 Hz to 10 kHz. Time interval between the repeated measurements was 2 min.

for the present purpose and a serious competitor of a superior, but more expensive substrate such as quartz. Anyway, the impedance level of a type-B sensor, described by, e.g., $\left|\underline{Z}(f = 20\,\text{Hz})\right|$, exceeds that of its type-A sensor counterpart by a factor of about 5.

Besides this, it can also be concluded from the curves in Fig. 10 that the response of the type-B and type-C sensors to hydrogen is similar. The respective reactances decrease by about 2 and 1 % in the two cases. We would not claim that type-B sensors systematically respond to H_2 more strongly than type-C sensors. Aging and other effects like fabrication tolerances of the layer thicknesses could have a non-negligible impact on the sensor response.

We assume that the influence of the more conductive substrates (type-A) are caused by the ionic conductivity of the glass at elevated temperatures. For type-B sensors the amount of insulating SiO_2 suffice to disrupt this type of conductivity through the substrate. Quartz (type-C) is considered to be a nearly ideal insulator. We assume that the small differences between type-B and type-C substrates are caused by impurities in the insulating SiO_2 layer which enables a minimum of ionic conductivity through the glass substrate.

5 Conclusion

We have demonstrated experimentally that the substrate plays an essential role for the overall performance of planar H_2 sensors involving TiO_2 / SnO_2 thin films. Aspects of

the impedance spectrum (the inflexion frequency) of high-conductivity substrates (like glass, an ion conductor at elevated temperatures) strongly depend on temperature and could therefore be used to recognize even small variations of the temperature.

Numerical experiments showed that high-conductivity substrates like glass can dominate the overall sensor response (impedance change) by 97 % at a frequency of 10.3 Hz. But a thin layer of SiO_2 (200 nm) suffices to increase the impedance level. Thereby just about 25 % of the impedance increase is hidden by the substrate influence. Only sensors based on a highly insulating substrate like quartz can excel this.

Thin-film gas sensors do not need special properties of the substrate (like crystallinity) except the compatibility with thin-film technology and mechanical stability. Hence, there is no need to use expensive substrates such as quartz. By depositing silicon dioxide on top of the substrate, even inexpensive substrates like glass can be made to work.

Sensors with both conducting substrate plus insulating thin film and insulating substrate respond to H_2 very similarly. Therefore, it can be excluded that the tested substrates influence the sensing mechanism in an unacceptable manner. Furthermore, neither the test bed nor the sensors showed a cross-sensitivity to humidity.

References

Barsan, N. and Weimar, U.: Conduction Model of Metal Oxide Gas Sensors, J. Electroceram., 7, 143–167, doi:10.1023/A:1014405811371, 2001.

Barsan, N., Koziej, D., and Weimar, U.: Metal oxide-based gas sensor research: How to?, Sensor. Actuat. B-Chem., 121, 18–35, doi:10.1016/j.snb.2006.09.047, 2007.

Fischerauer, A. and Fischerauer, G.: Physikalisches Modell der Materialparameterabhängigkeit des Impedanzspektrums planarer Chemosensoren in Mehrschichtbauweise, tm – Technisches Messen, 78, 15–22, doi:10.1524/teme.2011.0074, 2011.

Fischerauer, A., Schwarzmüller, Ch., and Fischerauer, G.: Substrate influence on the characteristics of interdigital-electrode gas sensors, Proc. Sixth Int'l Multi-Conf. on Systems, Signals & Devices (SSD'09), Djerba, 5 pp., doi:10.1109/ssd.2009.4956738, 23–26 March, 2009.

Fischerauer, A., Fischerauer, G., Hagen, G., and Moos, R.: Integrated impedance based hydro-carbon gas sensors with Na-zeolite/Cr2O3 thin-film interfaces: From physical modeling to devices, Phys. Status Solidi A, 208, 404–415, doi:10.1002/pssa.201026606, 2011.

Mardare, D., Iftime, N., and Luca, D.: TiO$_2$ thin films as sensing gas materials, J. Non-Cryst. Solids, 354, 4396–4400, doi:10.1016/j.jnoncrysol.2008.06.058, 2008.

Simon, I., Bârsan, N., Bauer, M., and Weimar, U.: Micromachined metal oxide gas sensors: opportunities to improve sensor performance, Sensor. Actuat. B-Chem., 73, 1–26, doi:10.1016/S0925-4005(00)00639-0, 2001.

Varghese, O. K., Gong, D., Paulose, M., Ong, K. G., and Grimes, C. A.: Hydrogen sensing using titania nanotubes, Sensor. Actuat. B-Chem., 93, 338–344, doi:10.1016/S0925-4005(03)00222-3, 2003.